Synthesis and characterisation of iodobismuthates containing N- substituted 1,4-diazabicyclo[2.2.2]octane

Journal of Chemical Crystallography
https://doi.org/10.1007/s10870-022-00957-x

ORIGINAL PAPER

Synthesis and Characterisation of Iodobismuthates Containing *N*-substituted 1,4-Diazabicyclo[2.2.2]octane

Yunhe Cai[1] · **Ann M. Chippindale**[1] · **Paz Vaqueiro**[1]

Received: 22 April 2022 / Accepted: 7 July 2022

Abstract

Two new hybrid iodobismuthates, $[C_8H_{17}N_2][C_{10}H_{22}N_2][BiI_6]$ (**1**) and $[C_6H_{12}N_2]_{0.5}[C_{10}H_{22}N_2]_{3.5}[Bi_2I_{10}][Bi_2I_9]$ (**2**), have been prepared by solvothermal synthesis in the presence of 1,4-diazabicyclo[2.2.2]octane (DABCO) and ethanol. Both compounds have been characterized by single-crystal and powder X-ray diffraction, infrared and UV–Vis spectroscopies and thermogravimetric analysis. Structure determination reveals that the crystal structure of **1** contains mononuclear $[BiI_6]^{3-}$ anions, whilst **2** contains an unusual combination of dinuclear anions, $[Bi_2I_9]^{3-}$ and $[Bi_2I_{10}]^{4-}$, consisting of two edge- and two face-sharing $[BiI_6]^{3-}$ octahedra, respectively. Mono- and diethylated derivatives of DABCO, which are formed in situ under solvothermal conditions, act as countercations and are located between the discrete anions. The optical band gaps of **1** and **2**, which are 2.29(1) and 2.03(2) eV respectively, are consistent with the red color of these compounds, and are comparable to the band gaps measured for other iodobismuthates containing discrete anions.

Graphical Abstract

Two new iodobismuthates, $[C_8H_{17}N_2][C_{10}H_{22}N_2][BiI_6]$ (**1**) and $[C_6H_{12}N_2]_{0.5}[C_{10}H_{22}N_2]_{3.5}[Bi_2I_{10}][Bi_2I_9]$ (**2**), have been synthesized under solvothermal conditions, and their crystal structures determined by single-crystal X-ray diffraction.

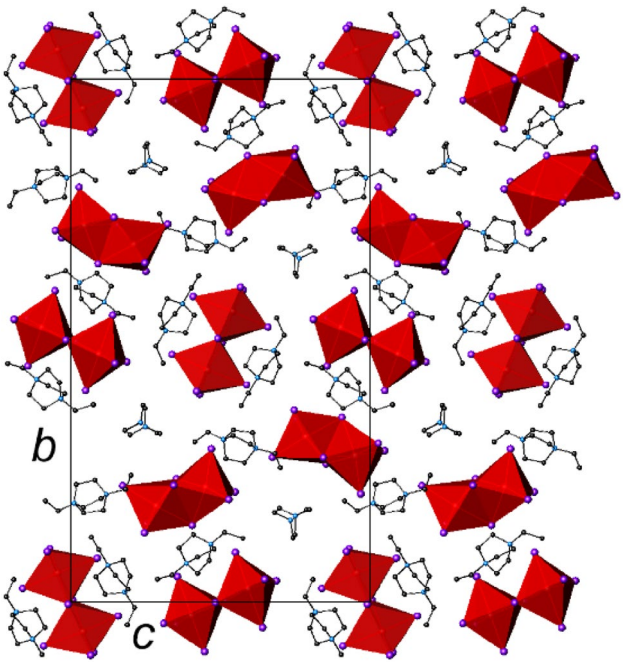

Keywords Iodidobismuthate · DABCO · Crystal structure · Semiconductor

Extended author information available on the last page of the article

Published online: 23 July 2022

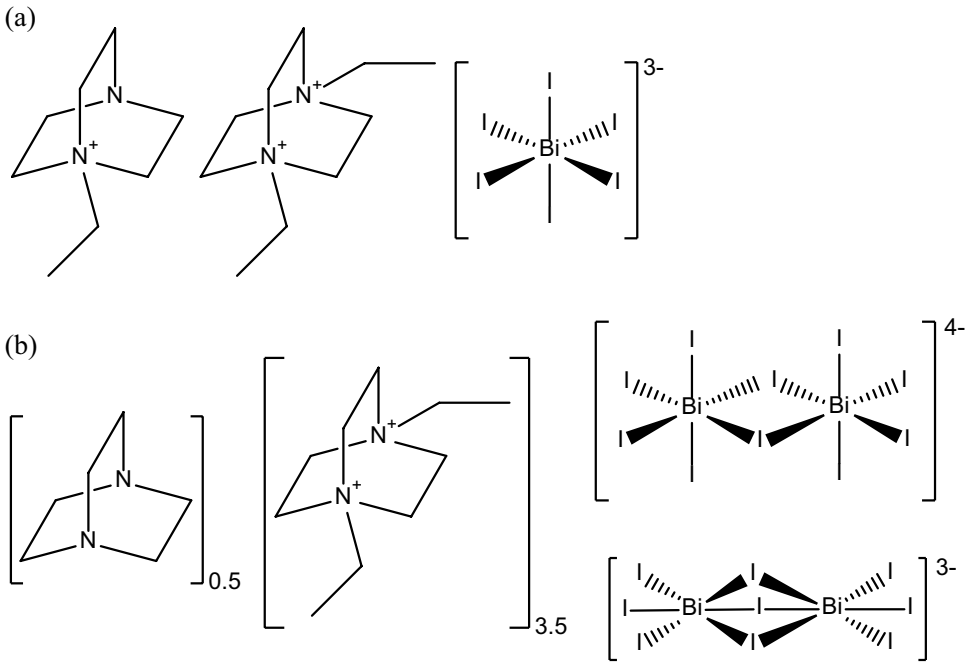

Scheme 1 Chemical structure diagram of (**a**) $[C_8H_{17}N_2][C_{10}H_{22}N_2][BiI_6]$ (**1**) and (**b**) $[C_6H_{12}N_2]_{0.5}[C_{10}H_{22}N_2]_{3.5}[Bi_2I_{10}][Bi_2I_9]$ (**2**)

Introduction

As an important class of low-dimensional hybrid materials, organic–inorganic halides of the type $R_xM_yX_z$ (where R is a protonated amine, M is a main-group metal and X is a halide) have attracted considerable interest, due to their structural diversity and optical and electronic properties [1, 2]. This class of materials is exemplified by the lead perovskite $MAPbI_3$ (where $MA = CH_3NH_3^+$). $MAPbI_3$ has been found to be a remarkable photovoltaic material [3–5], which when used in single-junction solar cells has a conversion efficiency of 25% [6], comparable to those of commercial silicon-based solar cells. Given the lower toxicity of bismuth when compared to that of its neighbors in the periodic table [7], bismuth-based organic–inorganic halides, which show better stability under ambient atmosphere than lead perovskites, are attracting interest as environmentally friendly materials for optoelectronic applications [8–10].

In hybrid iodobismuthates, the Bi^{3+} cation usually adopts a distorted octahedral coordination, with BiI_6 octahedra linked by vertex-, edge- or face-sharing into polynuclear anions [11–16]. A variety of polymeric, discrete polynuclear and mononuclear anionic units have been described previously [17]. The structures of the iodobismuthate anions formed are dependent on the size and shape of the organic countercations, as well as the synthetic conditions used [18, 19]. Protonated 1,4-diazabicyclo[2.2.2]octane (DABCO) and its *N*-substituted derivatives have been found to act as countercations in a number of iodobismuthates, as exemplified by $[C_6H_{14}N_2]_2[Bi_4I_{16}]\cdot 2H_2O$ [20] and $[Et_2DABCO]_2[Bi_2I_{10}]$ (where $[Et_2DABCO]^{2+}$ = *N*,*N*′-diethyl-1,4-diazabicyclo[2.2.2]octane) [21]. Most DABCO-containing iodobismuthates have been prepared solvothermally, in the presence of hydroiodic acid, and consist of discrete anions, including mononuclear $[BiI_6]^{3-}$ [22], dimeric $[Bi_2I_9]^{3-}$ and $[Bi_2I_{10}]^{4-}$ [21, 23], and tetrameric $[Bi_4I_{16}]^{4-}$ units [20]. When $[Me_2DABCO]I_2$ is used as a reagent (where $[Me_2DABCO]^{2+}$ = *N*,*N*′-dimethyl-1,4-diazabicyclo[2.2.2] octane), one-dimensional chains with stoichiometry $[Bi_2I_{10}]^{4-}$ are produced [21]. We have recently shown that, in the absence of hydroiodic acid in solvothermal reactions, DABCO can also act as a linker, as exemplified by $(C_6H_{12}N_2)BiI_3$, in which pairs of edge-sharing bismuth octahedra are linked by DABCO ligands into hybrid ribbons [24].

Here, we describe the solvothermal synthesis and characterization of two new hybrid iodobismuthates containing N-substituted DABCO (Scheme 1). $[C_8H_{17}N_2][C_{10}H_{22}N_2][BiI_6]$ (**1**) contains mononuclear $[BiI_6]^{3-}$ anions, while $[C_6H_{12}N_2]_{0.5}[C_{10}H_{22}N_2]_{3.5}[Bi_2I_{10}][Bi_2I_9]$ (**2**) contains an unusual combination of dinuclear anions, $[Bi_2I_9]^{3-}$ and $[Bi_2I_{10}]^{4-}$.

Experimental Section

All compounds were synthesized in 23 mL Teflon-lined stainless-steel autoclaves. Ethanol (> 99.8%), BiI_3 (99%), AgI (99.9%), KI (≥ 99%), and DABCO (≥ 99%) were obtained from Sigma-Aldrich. For each reaction, the reagents were loaded into the Teflon liner and stirred for approximately 10 min, prior to the reaction vessel being sealed into the autoclave and heated. The heating and cooling rates were 0.83 °C min^{-1}. After cooling to room temperature, the products were collected by vacuum filtration and washed with ethanol and deionized water.

Synthesis of $[C_8H_{17}N_2][C_{10}H_{22}N_2][BiI_6]$ (1)

BiI_3 (0.5860 g, 1 mmol), KI (0.1677 g, 1 mmol), DABCO (0.1401 g, 1.25 mmol) and ethanol (10 mL) were heated in the sealed autoclave at 170 °C for 5 days. The solid product consisted of a small amount of a dark powder, identified by powder X-ray diffraction as bismuth metal, and red crystals of **1**. Elemental analysis of hand-picked crystals of **1**: C = 16.95%, H = 2.95%, N = 4.39%; calc for $[C_8H_{17}N_2][C_{10}H_{22}N_2][BiI_6]$: C = 16.84%, H = 3.04%, N = 4.36%.

Synthesis of $[C_6H_{12}N_2]_{0.5}[C_{10}H_{22}N_2]_{3.5}[Bi_2I_{10}][Bi_2I_9]$ (2)

Initially, this compound was prepared by heating BiI_3 (0.5913 g, 1 mmol), AgI (0.2390 g, 1 mmol), KI (0.3365 g, 2 mmol), DABCO (0.1225 g, 1 mmol) and ethanol (10 mL) at 170 °C for 5 days. The solid product consisted of red needles of **2**, bismuth powder, and a small amount of an unidentified impurity in the form of red blocks. Subsequently, compound **2** was prepared in the absence of AgI, using a reaction mixture with a molar ratio of 1:1.75:0.75 of Bi:KI:DABCO, heated at 170 °C for 5 days. Elemental analysis of hand-picked crystals of **2**: C = 12.52%, H = 2.16%, N = 3.06%; calc for $[C_6H_{12}N_2]_{0.5}[C_{10}H_{22}N_2]_{3.5}[Bi_2I_{10}][Bi_2I_9]$: C = 11.71%, H = 2.15%, N = 2.87%.

Single-Crystal X-ray Diffraction

Single-crystal X-ray diffraction data (Table 1) were collected using Mo Kα radiation (λ = 0.71073 Å) using an Agilent Gemini S Ultra diffractometer for **1** and a Rigaku XtaLAB Synergy diffractometer for **2**. Preliminary data for the impurity present in the bulk sample of compound **2** were collected at the UK National Crystallography Service (Southampton, UK) [25] using a Rigaku XtaLAB Diffractometer with an AFC12 goniometer and a rotating anode Mo source. Data reduction was carried out in each case using CrysAlisPro [26]. The structures were solved using Superflip [27] and refined against *F* using the program CRYSTALS [28]. The crystal of **1**, solved in space group $P2_13$, was found to be an inversion twin with a Flack parameter of 0.48(2). Although Platon/ADDSYM suggests $Pa\bar{3}$ as a possible space group for **1**, refinements in this space group were not successful. The crystal structure in this space group contains only a single DABCO moiety and attached ethyl groups could not be modelled satisfactorily. As described below, two distinct DABCO moieties, with one and two ethyl groups attached, are identified in the final structure in $P2_13$ and are necessary in order to achieve charge balance.

Data for compound **2** were treated with SQUEEZE [29] to correct for the effects of disordered organic cations. SQUEEZE found a total void volume of 423 Å per unit cell, which contained 45 electrons. This is consistent with the presence of half a $[Et_2DABCO]^{2+}$ moiety per unit cell (48 electrons).

Table 1 Crystallographic data for compounds **1** and **2**

Compound	**1**	**2**
Crystallographic formula	$C_{18}H_{39}N_4BiI_6$	$C_{33}H_{72}N_7Bi_4I_{19}$
*M*r	1281.94	3814.09
Crystal habit	Red block	Red needle
Crystal system	Cubic	Monoclinic
T/K	150	100
Space group	$P\,2_13$	$P\,2_1/c$
a/Å	14.9269(3)	8.95779(1)
b/Å	14.9269(3)	40.19181(2)
c/Å	14.9269(3)	22.98174(2)
α/°	90	90
β/°	90	93.166(2)
γ/°	90	90
Cell volume/Å^3	3325.9(2)	8261.483(19)
Z	4	4
ρ_{cal}/g cm^{-3}	2.560	3.066
R_{int}	0.0431	0.0546
R^a (I > 3.0σ(I))	0.0412	0.0322
Rw^b	0.0420	0.0263
GoF	1.339	0.8620

[a] $R(F_o) = \sum(|F_o| - |F_c|)/\sum|F_o|$

[b] $R_w(F_o) = [\sum w(|F_o| - |F_c|)^2/\sum w|F_o|^2]^{1/2}$

Characterization

Powder X-ray diffraction patterns were collected at room temperature for the as-synthesized materials and for finely-ground hand-picked crystals of **1** and **2** using a Bruker D8 Advance powder X-ray diffractometer (Cu $K_{\alpha 1}$ radiation, λ = 1.5406 Å). Pawley refinements were performed within Topas [30] in order to confirm the identity of the crystals formed in the two reactions.

Additional characterization measurements were carried out on ground hand-picked crystals of **1** and **2**. Thermogravimetric Analysis (TGA) was performed on a TA-TGA Q50 instrument, operating under a flowing nitrogen atmosphere. Data were collected from room temperature to 650 °C, at a rate of 10 °C/min. UV–Vis diffuse reflectance data were collected using a Perkin Elmer Lambda 35 UV–Vis spectrometer equipped with an integrating sphere and using $BaSO_4$ as a standard. The absorption data were calculated using the Kubelka–Munk function [31]. Fourier Transform infrared spectra were collected using a Perkin Elmer Spectrum 100 FT-IR spectrometer. Elemental analysis was carried out by MEDAC LTD.

Results and Discussion

Analysis of the powder X-ray diffraction data for the as-synthesized products of the reactions described above indicates that, in addition to compounds **1** and **2**, bismuth metal is always present (Supplementary Information), indicating that these reactions involve redox processes. In the case of the reaction producing **2**, the solid product also contained a small amount of an unidentified impurity. Preliminary single-crystal diffraction data collected on this impurity indicates that it crystallises in the space group $P\ 2_1/c$, with lattice parameters $a = 9.0406(1)$, $b = 16.0735(2)$, $c = 34.1517(6)$ Å and $\beta = 92.1522(13)°$. Attempts to produce larger amounts of this impurity, to enable its full characterization, have so far been unsuccessful.

As illustrated in Fig. 1, there is good agreement between the experimental and calculated powder X-ray patterns, based on the structures determined for these compounds using single-crystal X-ray diffraction. The lattice parameters determined from the powder diffraction data agree well with those determined by single-crystal diffraction (Supplementary Information). FTIR data collected on handpicked crystals of **1** and **2** (Supplementary Information) are in good agreement with previous literature reports for DABCO [32, 33], confirming its presence in the products. At high wavenumbers, the absorption centered at around 2900 cm^{-1} is assignable to CH_2 stretches, while bands at 1300–1500 cm^{-1} can be associated with the CH_2 deformation (δ) and CH_2 deformation (t-w) modes.

Crystal Structure of $[C_8H_{17}N_2][C_{10}H_{22}N_2][BiI_6]$ (1)

The asymmetric unit of **1** (Supplementary Information) contains one third of a $[BiI_6]^{3-}$ octahedron, and one third of two *N*-substituted DABCO cations. Although the reagents used were DABCO and ethanol, an alkylation reaction has taken place under the solvothermal conditions, and the product of this reaction contains ethylated DABCO cations. In-situ alkylation reactions have been previously observed in solvothermal reactions involving amines and alcohols [24, 34]. In the cubic crystal structure of **1**, the $[BiI_6]^{3-}$ anions and the DABCO moieties are located on crystallographic threefold axes, while the ethyl chains on the DABCO moieties are disordered around the threefold axes. Charge balancing considerations require the presence of one $[EtDABCO]^+$ and one $[Et_2DABCO]^{2+}$ cation per formula unit, and the elemental analysis is in excellent agreement with the proposed formula, $[Et_2DABCO]^{2+}[EtDABCO]^+[BiI_6]^{3-}$.

In the distorted $[BiI_6]^{3-}$ octahedron found in **1**, the Bi–I bond distances are 3.040(2) and 3.121(2) Å. The I–Bi–I angles range between 88.52(5) and 92.62(7)°, a small but

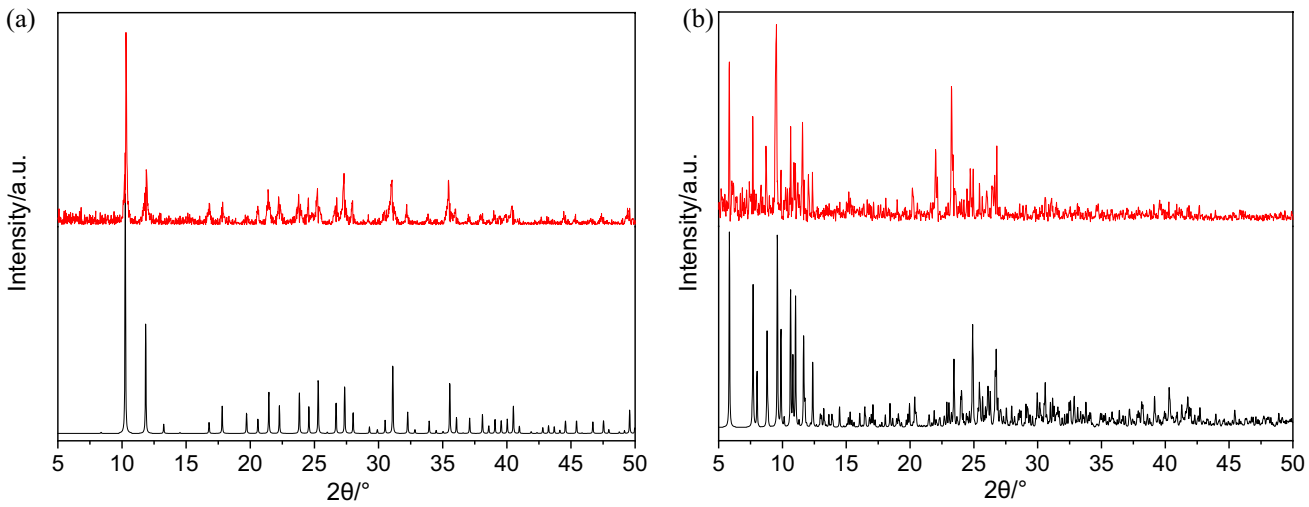

Fig. 1 Experimental powder X-ray diffraction patterns (red line) collected for handpicked crystals from the reactions producing (**a**) **1** and (**b**) **2**. The patterns calculated using the structures determined by single-crystal X-ray diffraction are shown in black (Color figure online)

significant deviation from ideal octahedral geometry. The mononuclear $[BiI_6]^{3-}$ anion is relatively rare when compared with discrete polynuclear anions [17, 18]. Similar octahedral $[BiI_6]^{3-}$ anions have been previously found in $[C(NH_2)_3]_3[BiI_6]$ [35], $[CH_3CH_2NH_3]_3[BiI_6]$ [36], $[TTF]_4[BiI_6]$ (where TTF = tetrathiafulvalene) [37] and $[Et_2DABCO]_3[BiI_6]_2$ [22], while $[H_3N–R–NH_3]_2[I_3][BiI_6]$ [38, 39] and $[C_6H_{13}N]_4[I_3][BiI_6]$ [40] contain two types of anions; namely $[BiI_6]^{3-}$ units and triiodide, I_3^-, ions.

In the crystal structure of **1** (Fig. 2a), each $[BiI_6]^{3-}$ anion is surrounded by eight $[Et_2DABCO]^{2+}$ cations. Figure 2b shows a slice of the crystal structure, parallel to the (010) planes, in which each $[BiI_6]^{3-}$ anion is surrounded by two diethylated and two monoethylated DABCO cations in the same plane. Two additional ethylated DABCO cations are located above each $[BiI_6]^{3-}$ anion, and two below. There are no short I···I distances (below the van der Waals' radii for two iodine atoms, 3.96 Å) [41], between the $[BiI_6]^{3-}$ anions. Instead, there are a number of short C–H···I contacts (Supplementary Information), which are likely to contribute to the stabilization of this crystal structure.

Crystal Structure of $[C_6H_{12}N_2]_{0.5}[C_{10}H_{22}N_2]_{3.5}[Bi_2I_{10}][Bi_2I_9]$ (2)

Compound **2**, $[C_6H_{12}N_2]_{0.5}[C_{10}H_{22}N_2]_{3.5}[Bi_2I_{10}][Bi_2I_9]$, which crystallizes in the monoclinic space group $P2_1/c$, contains two types of dimeric anions, $[Bi_2I_9]^{3-}$ and $[Bi_2I_{10}]^{4-}$ (Fig. 3a). The coexistence of two types of dimeric anions in the structure of iodobismuthates is quite unusual, with only one previous example containing $[Bi_2I_9]^{3-}$ and $[Bi_2I_{10}]^{4-}$, $[MV]_5[Bi_2I_{10}][Bi_2I_9]_2$ (where MV^{2+} = methyl viologen) [42], reported to date. The $[Bi_2I_9]^{3-}$ and $[Bi_2I_{10}]^{4-}$ anions are formed by two $[BiI_6]^{3-}$ octahedra which share a face or an edge, respectively (Fig. 3a). In $[Bi_2I_9]^{3-}$, the two Bi^{3+} cations are bridged by three iodides, with each Bi^{3+} cation additionally coordinated by three terminal iodides. The Bi–I bond lengths lie between 2.9619(4) and 3.2190(4) Å, with the Bi–I distances for the bridging μ_2-I^- anions being significantly longer than those for the terminal iodides. These distances are comparable to those found in other iodobismuthates containing $[Bi_2I_9]^{3-}$ dimers, including $[C_9H_{17}N_2]_3[Bi_2I_9]$ [43] and $[Me_2DABCO]_7[BiI_6]_2[Bi_2I_9]_2{\cdot}2I_3$ [23]. In the $[Bi_2I_{10}]^{4-}$ dimers, which contain two bridging μ_2-I^-, the Bi-I bond distances vary between 2.9515(4) and 3.2597(4) Å while the I–Bi–I angles range from 80.401(9)° to 99.599(9)°. These values are similar to those found in

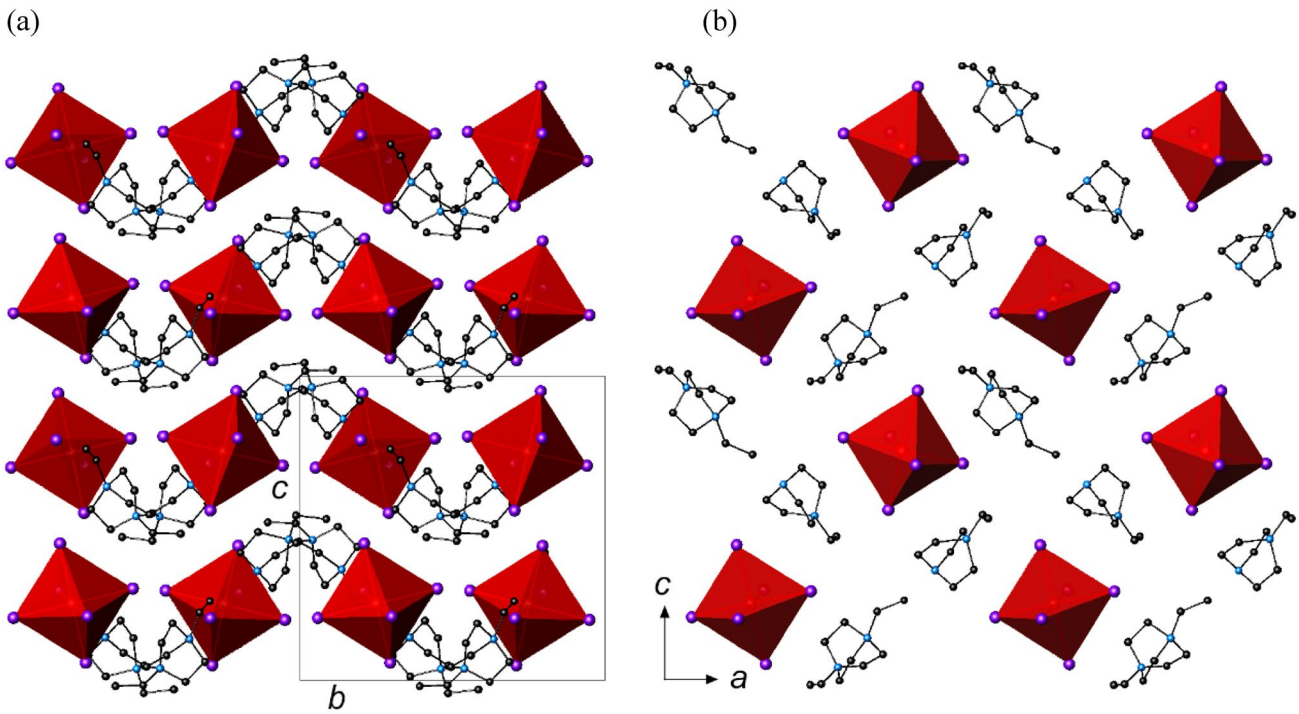

Fig. 2 (**a**) Polyhedral view of the crystal structure of $[C_8H_{17}N_2][C_{10}H_{22}N_2][BiI_6]$ (**1**). The unit cell is shown. Only one orientation of the disordered ethyl chains is shown. (**b**) Polyhedral view of one slice of **1**, parallel to the (010) planes. Hydrogen atoms have been omitted for clarity. Key: bismuth, large red spheres; iodine, large purple spheres; carbon, small black spheres; nitrogen, small blue spheres; bismuth centered-octahedra are shown in red (Color figure online)

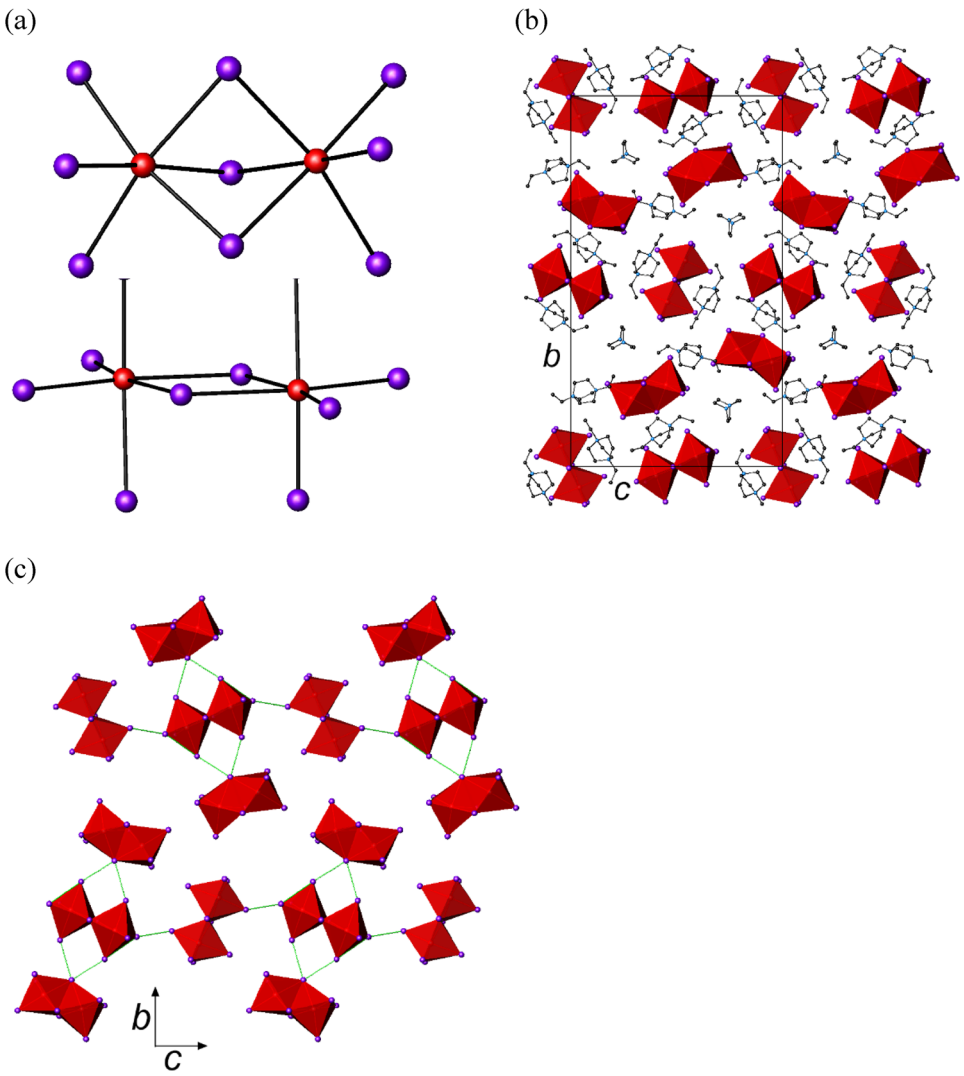

Fig. 3 (**a**) The $[Bi_2I_9]^{3-}$ (upper) and $[Bi_2I_{10}]^{4-}$ (lower) anions found in **2**. (**b**) View of the crystal structure of **2** along [100] with unit cell outlined showing the locations of the DABCO and $[Et_2DABCO]^{2+}$ species. Hydrogen atoms have been omitted for clarity. (**c**) Short I···I contacts (green lines) are shown between the $[Bi_2I_9]^{3-}$ and $[Bi_2I_{10}]^{4-}$ anions, viewed along [100]. Organic cations have been omitted for clarity. Key as for Fig. 1 (Color figure online)

other compounds containing dimeric $[Bi_2I_{10}]^{4-}$ anions, such as $[Et_2DABCO]_2[Bi_2I_{10}]$ [21].

The crystallographically-determined formula for compound **2** is $[DABCO]_{0.5}[Et_2DABCO]^{2+}{}_3[Bi_2I_{10}]^{4-}[Bi_2I_9]^{3-}$. Charge balancing considerations require the incorporation of three and a half $[Et_2DABCO]^{2+}$ cations per formula unit. Although only three $[Et_2DABCO]^{2+}$ cations were located in the crystal structure by single-crystal X-ray diffraction, there is a significant amount of void space (423 Å per unit cell), where half an $[Et_2DABCO]^{2+}$ moiety per unit cell could be accommodated. Elemental analysis is consistent with the proposed formula for **2**, which is $[DABCO]_{0.5}[Et_2DABCO]^{2+}{}_{3.5}[Bi_2I_{10}]^{4-}[Bi_2I_9]^{3-}$. In the crystal structure of **2**, layers of $[Bi_2I_9]^{3-}$ anions and layers of $[Bi_2I_{10}]^{4-}$ anions, separated by the organic moieties, alternate along the [010] direction (Fig. 3b). There are a number of I···I contacts between the anions over the range 3.91 to 4.19 Å (Supplementary Information), comparable to the sum of the van der Waals' radii for two iodine atoms [41], which link the discrete anions into a pseudo-two-dimensional structure (Fig. 3c). It has been suggested that in crystal structures containing discrete iodobismuthate anions, the presence of I···I contacts might lead to increased band dispersion, particularly when the I···I distances are comparatively short [44]. In addition to the I···I contacts, in the crystal structure of **2** there are also many short C–H···I distances at under 3.4 Å, which are also likely to stabilize the crystal structure.

Thermal Stability and UV–Vis Diffuse Reflectance

Thermogravimetric data (Fig. 4a) indicate that, under a nitrogen atmosphere, both compounds are stable up to approximately 280 °C, with decomposition occurring in each case in a single step. UV–Vis diffuse reflectance data collected on ground crystals of **1** and **2** are shown in Fig. 4b. Absorption peaks observed at approximately 2.6 and 2.3 eV for **1** and **2,** respectively, might be attributed to an exciton. These are often observed in the UV–Vis absorption spectra

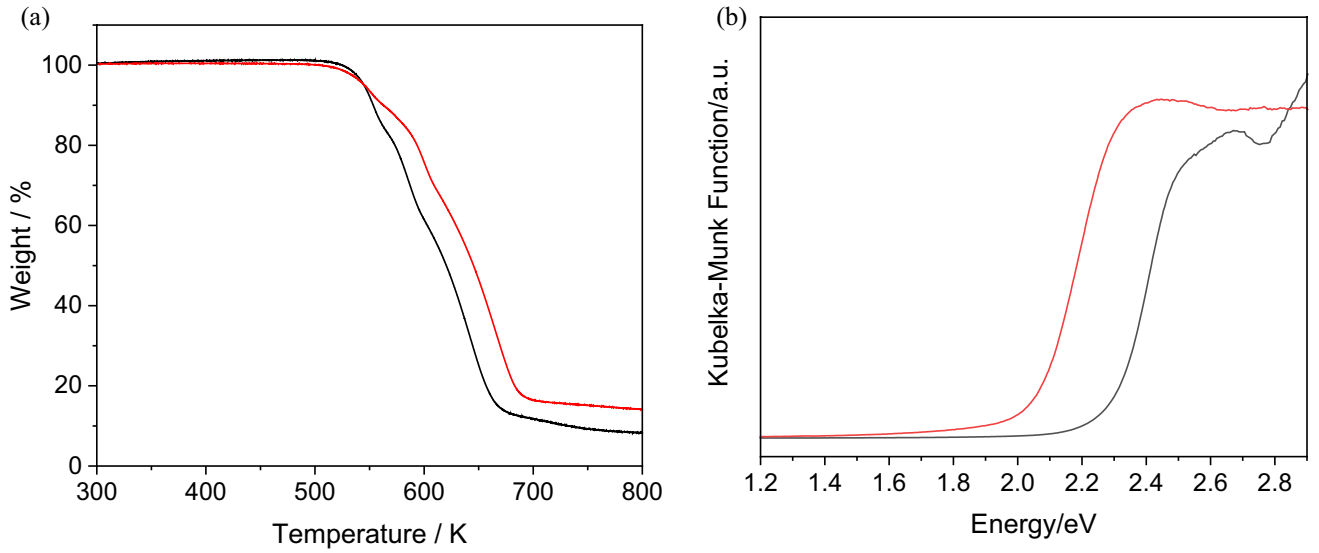

Fig. 4 (**a**) TGA data and (**b**) UV–Vis diffuse reflectance data for compounds **1** (black) and **2** (red) (Color figure online)

Table 2 Optical band gaps for selected iodobismuthates

Formula	Band gap/eV	Ref.
$[C_8H_{17}N_2][C_{10}H_{22}N_2][BiI_6]$ (**1**)	2.29	This work
$[Et_2DABCO]_3[BiI_6]_2$	2.24	[22]
$[C_3H_{10}N]_3[BiI_6]$	2.1	[39]
$[C_3H_{10}N]_4[I_3][BiI_6]$	1.34	[39]
$[C_6H_{13}N]_4[I_3][BiI_6]$	1.58	[40]
$[C_6H_{12}N_2]_{0.5}[C_{10}H_{22}N_2]_{3.5}[Bi_2I_{10}][Bi_2I_9]$ (**2**)	2.03	This work
$[C_6H_{14}N]_3[Bi_2I_9]$	2.02	[40]
$[MA]_3[Bi_2I_9]$	2.0–2.1	[47, 48]
$[C_8H_{12}N]_3[Bi_2I_9]$	2.38	[49]
$[(CH_3)_3NH]_3[Bi_2I_9]$	2.0	[50]
$[C_9H_7N_2]_3[Bi_2I_9]$	2.1	[43]
$[Me_2DABCO]_7(BiI_6)_2(Bi_2I_9)_2\ 2I_3$	1.61	[23]
$[C_9H_{14}N_4]_2[Bi_2I_{10}]$	1.9	[51]
$[i\text{-}Pr_2DABCO]_2[Bi_2I_{10}]$	1.73	[22]
$[Et_2DABCO]_2[Bi_2I_{10}]$	2.10	[21]
$[Pr_2DABCO]_2[Bi_2I_{10}]$	2.16	[21]

of iodobismuthates, even when measurements are performed at room temperature [45, 46].

From the absorption edge, the optical band gap of **1**, which contains mononuclear $[BiI_6]^{3-}$ anions, is estimated as 2.29(1) eV, while **2**, which contains dinuclear $[Bi_2I_9]^{3-}$ and $[Bi_2I_{10}]^{4-}$ units, exhibits a band gap estimated as 2.03(2) eV. Comparison with previously reported band gaps for iodobismuthates containing only either mononuclear [22, 39, 40] or dinuclear $[Bi_2I_9]^{3-}$ [23, 40, 43, 47–50] and $[Bi_2I_{10}]^{4-}$ [21, 22, 51] anions (Table 2) reveals that the optical band gap is largely independent of the nature of the organic countercations. The band gaps of hybrid iodobismuthates are mainly determined by the inorganic moieties, because the main contributors to the top of the valence band are iodine 5*p* states, while the bottom of the conduction band is primarily formed by bismuth 6*p* states [44]. Incorporation of triiodide anions has been successfully exploited to achieve significant reductions in band gap, as exemplified by $[C_3H_{10}N]_4[I_3][BiI_6]$ [39] and $[Me_2DABCO]_7(BiI_6)_2(Bi_2I_9)_2{\cdot}2I_3$ [23] (Table 2). Lower optical band gaps have also been found for polymeric bismuth iodides, which are comparatively rare. Examples include $[MV][BiI_5]$ (where MV^{2+} = methyl viologen), which contains one-dimensional chains of corner-sharing $[BiI_6]^{3-}$ octahedra and exhibits a band gap of 1.48 eV [34], and $[C_3H_5N_2S][BiI_4]$, which has a band gap of 1.78 eV and contains one-dimensional chains of edge-sharing octahedra [52]. Incorporation of additional metals to form ternary iodobismuthates, such as $[HPy]_2[Py][CuBi_3I_{12}]$ (where Py = pyridine) which has a band gap of 1.59 eV [53], may provide an alternative approach to achieve significant reductions in the band gap [54].

Conclusions

In summary, two new iodobismuthates have been synthesized under solvothermal conditions in the presence of DABCO and ethanol, and their crystal structures determined by single-crystal X-ray diffraction. Although we have previously shown that DABCO can act as a linker between iodobismuthate moieties [24], in-situ alkylation of DABCO is occurring under the solvothermal conditions described here. Compounds **1** and **2** contain discrete mononuclear and dinuclear anions, rather than polymeric units, and exhibit

optical band gaps comparable to those of other iodobismuthates containing discrete anions.

Supplementary Information The online version contains supplementary material available at https://doi.org/10.1007/s10870-022-00957-x.

Acknowledgements The University of Reading is acknowledged for access to the Chemical Analysis Facility. Mr Nick Spencer is thanked for his assistance with the collection of single-crystal X-ray diffraction data and Dr Pedro Rivas Ruiz for help with FT-IR and Thermogravimetric Analysis.

Funding No funding was received for conducting this study.

Data Availability All data generated or analyzed for this work are included in the article and the Supplementary Information document. CCDC numbers 2167555 and 2167557 contain the crystallographic data for compounds **1** and **2** reported in this paper. These data can be obtained free of charge via www.ccdc.cam.ac.uk/data_request/cif, or by emailing data_request@ccdc.cam.ac.uk, or by contacting The Cambridge Crystallographic Data Centre, 12 Union Road, Cambridge CB2 1EZ, UK; fax: +44 1223 336033.

Declarations

Conflict of interest The authors have no conflict of interest to declare that are relevant to the content of this paper.

References

1. Klejna S, Mazur T, Wlazlak E, Zawal P, Soo HS, Szaciłowski K (2020) Halogen-containing semiconductors: from artificial photosynthesis to unconventional computing. Coord Chem Rev 415:213316. https://doi.org/10.1016/j.ccr.2020.213316
2. Saparov B, Mitzi DB (2016) Organic–inorganic perovskites: structural versatility for functional materials design. Chem Rev 116:4558–4596. https://doi.org/10.1021/acs.chemrev.5b00715
3. Kojima A, Teshima K, Shirai Y, Miyasaka T (2009) Organometal halide perovskites as visible-light sensitizers for photovoltaic cells. J Am Chem Soc 131:6050–6051. https://doi.org/10.1021/ja809598r
4. Cao DH, Stoumpos CC, Farha OK, Hupp JT, Kanatzidis MG (2015) 2D homologous perovskites as light-absorbing materials for solar cell applications. J Am Chem Soc 137:7843–7850. https://doi.org/10.1021/jacs.5b03796
5. Stoumpos CC, Cao DH, Clark DJ, Young J, Rondinelli JM, Jang JI, Hupp JT, Kanatzidis MG (2016) Ruddlesden-Popper hybrid lead iodide perovskite 2D homologous semiconductors. Chem Mater 28:2852–2867. https://doi.org/10.1021/acs.chemmater.6b00847
6. Min H, Lee DY, Kim J, Kim G, Lee KS, Kim J, Paik MJ, Kim YK, Kim KS, Kim MG, Shin TJ, Il Seok S (2021) Perovskite solar cells with atomically coherent interlayers on SnO_2 electrodes. Nature 598:444–450. https://doi.org/10.1038/s41586-021-03964-8
7. Yang N, Sun H (2011) Bismuth: environmental pollution and health effects. Encycl Environ Health. https://doi.org/10.1016/B978-0-444-52272-6.00374-3
8. Pious JK, Muthu C, Vijayakumar C (2022) Organic spacer cation assisted modulation of the structure and properties of bismuth halide perovskites. Acc Chem Res 55:275–285. https://doi.org/10.1021/acs.accounts.1c00545
9. Wu C, Zhang Q, Liu G, Zhang Z, Wang D, Qu B, Chen Z, Xiao L (2019) From Pb to Bi: A promising family of Pb-free optoelectronic materials and devices. Adv Energy Mater 10:1902496. https://doi.org/10.1002/aenm.201902496
10. Zhang L, Wang K, Zou B (2019) Bismuth halide perovskite-like materials: current opportunities and challenges. Chemsuschem 12:1612–1630. https://doi.org/10.1002/cssc.201802930
11. Liu B, Xu L, Guo GC, Huang JS (2006) Three inorganic–organic hybrids of bismuth(III) iodide complexes containing substituted 1,2,4-triazole organic components with charaterizations of diffuse reflectance spectra. J Solid State Chem 179:1611–1617. https://doi.org/10.1016/j.jssc.2006.02.011
12. Goforth AM, Tershansy MA, Smith MD, Peterson L Jr, Kelley JG, DeBenedetti WJ, Zur Loye HC (2011) Structural diversity and thermochromic properties of iodobismuthate materials containing d-metal coordination cations: observation of a high symmetry $[Bi_3I_{11}]^{2-}$ anion and of isolated I^- anions. J Am Chem Soc 133:603–612. https://doi.org/10.1021/ja108278j
13. Hrizi C, Samet A, Abid Y, Chaabouni S, Fliyou M, Koumina A (2011) Crystal structure, vibrational and optical properties of a new self-organized material containing iodide anions of bismuth(III), $[C_6H_4(NH_3)_2]_2Bi_2I_{10}{\cdot}4H_2O$. J Mol Struct 992:96–101. https://doi.org/10.1016/j.molstruc.2011.02.051
14. Heine J (2015) A step closer to the binary: the $^1{}_\infty[Bi_6I_{20}]^{2-}$ anion. Dalton Trans 44:10069–10077
15. Usolt'sev AN, Shentseva IA, Shayapov VR, Plyusnin PE, Korol'kov IV, Sokolov MN, Adonin SA (2021) Bismuth(III) iodide complexes with 1-ethyl-4-dimethylaminopyridinium: structure, thermal stability, and optical properties. Russ J Inorg Chem 66:1482–1487
16. Adonin SA, Peresypkina EV, Sokolov MN, Fedin VP (2014) Trinuclear iodobismuthate complex $[Na_3(Me_2CO)_{12}][Bi_3I_{12}]$: synthesis and crystal structure. Russ J Inorg Chem 40:867–870
17. Wu LM, Wu XT, Che L (2009) Structural overview and structure–property relationships of iodoplumbate and iodobismuthate. Coord Chem Rev 253:2787–2804. https://doi.org/10.1016/j.ccr.2009.08.003
18. Adonin SA, Sokolov MN, Fedin VP (2016) Polynuclear halide complexes of Bi(III): from structural diversity to the new properties. Coord Chem Rev 312:1–21. https://doi.org/10.1016/j.ccr.2015.10.010
19. Adonin SA, Sokolov MN, Fedin VP (2017) Bismuth(III) halide complexes: new structural types and new application areas. Russ J Inorg Chem 62:1789–1796
20. Dennington AJ, Weller MT (2018) Synthesis, structure and optoelectronic properties of hybrid iodobismuthate & iodoantimonate semiconducting materials. Dalton Trans 47:3469–3484. https://doi.org/10.1039/C7DT04280A
21. Chen BG (2017) Organic/bismuth iodides hybrids: structural perturbation of substitutes and their photocurrent response properties. J Clust Sci 28:983–994. https://doi.org/10.1007/s10876-016-1089-5

22. Zhang ZP, Feng QY, Wei YL, Gao ZY, Wang ZW, Wang YM (2018) Three iodobismuthates hybrids displaying mono-nuclear, dimer and 1-D arrangements templated by 1,4-diazabicyclo[2.2.2]octane derivatives: semiconductor and photocurrent response properties. J Clust Sci 29:725–735. https://doi.org/10.1007/s10876-018-1397-z
23. Zhang ZP, Feng QY, Wang QL, Huang XY, Chen D, Zhou J (2018) A new iodobismuthate-based hybrid containing mixed iodobismuthate clusters templated by diammonium cation: structure and photocurrent response. J Clust Sci 29:367–374. https://doi.org/10.1007/s10876-018-1339-9
24. Cai Y, Chippindale AM, Curry RJ, Vaqueiro P (2021) Multiple roles of 1,4-diazabicyclo[2.2.2]octane in the solvothermal synthesis of iodobismuthates. Inorg Chem 60:5333–5342. https://doi.org/10.1021/acs.inorgchem.1c00318
25. Coles SJ, Gale PA (2012) Changing and challenging times for service crystallography. Chem Sci 3:683–689. https://doi.org/10.1039/C2SC00955B
26. Rigaku OD (2019) CrysAlisPRO. Oxford Diffraction, Rigaku Corporation, Oxford
27. Palatinus L, Chapuis G (2007) SUPERFLIP—a computer program for the solution of crystal structures by charge flipping in arbitrary dimensions. J Appl Cryst 40:786–790. https://doi.org/10.1107/S0021889807029238
28. Betteridge PW, Carruthers JR, Cooper RI, Prout K, Watkin DJ (2003) Crystals version 12: software for guided crystal structure analysis. J Appl Cryst 36:1487. https://doi.org/10.1107/S0021889803021800
29. Spek AL (2015) PLATON SQUEEZE: a tool for the calculation of the disordered solvent contribution to the calculated structure factors. Acta Cryst C71:9–18. https://doi.org/10.1107/S2053229614024929
30. TOPAS, Version 3. Bruker-AXS Inc, Madison, 1999.
31. Wendlandt WW, Hecht HG (1966) Reflectance spectroscopy. Interscience Publishers, New York
32. Marzocchi MP, Sbrana G, Zerbi G (1965) Structure and fundamental vibrations of cage molecules I. 1,4-diazabicyclo[2.2.2]octane. J Am Chem Soc 87:1429–1432. https://doi.org/10.1021/ja01085a003
33. Messina MT, Metrangolo P, Navarrini W, Radice S, Resnati G, Zerbi G (2000) Infrared and Raman analyses of the halogen-bonded non-covalent adducts formed by α, ω-diiodoperfluoroalkanes with DABCO and other electron donors. J Mol Struct 524:87–94. https://doi.org/10.1016/S0022-2860(99)00445-7
34. Wang Y, Wen R, Liu Y, Bi LY, Yang M, Sun H, Zheng YZ, Zhang G, Gao Z (2020) Rigid amine-induced pseudo-3 D lead-free bismuth halide perovskite with an improved band edge for visible-light absorption. Chemsuschem 13:2753–2760. https://doi.org/10.1002/cssc.202000282
35. Li SG, Chen L, Xiang Y (2017) Synthesis, crystal structures and characterization of two novel organic-inorganic hybrid compounds $(C_5NH_6)_6Bi_4Br_18$ and $[C(N_H2)_3]_3Bi_I6$. J Mol Struct 1130:617–622. https://doi.org/10.1016/j.molstruc.2016.11.025
36. Li HH, Wang CF, Wu YX, Jiang F, Shi C, Ye HY, Zhang Y (2020) Halogen substitution regulates the phase transition temperature and band gap of semiconductor compounds. Chem Commun 56:1697–1700. https://doi.org/10.1039/C9CC09477F
37. Evans HA, Labram JG, Smock SR, Wu G, Chabinyc ML, Seshadri R, Wudl F (2017) Mono- and mixed-valence tetrathiafulvalene semiconductors (TTF)BiI_4 and $(TTF)_4BiI_6$ with 1D and 0D bismuth-iodide networks. Inorg Chem 56:395–401. https://doi.org/10.1021/acs.inorgchem.6b02287
38. Bi W, Louvain N, Mercier N, Luc J, Sahraoui B (2007) Type structure, which is composed of organic diammonium, triiodide and hexaiodobismuthate, varies according to different structures of incorporated cations. CrystEngComm 9:298–303. https://doi.org/10.1039/B617178H
39. Zhang W, Kou B, Peng Y, Wu Z, Yao Y, Dey D, Li L, Luo J (2018) Rational design of a triiodide-intercalated dielectric-switching hybrid for visible-light absorption. J Mater Chem C 6:12170–12174. https://doi.org/10.1039/C8TC04372H
40. Zhang W, Liu X, Li L, Sun Z, Han S, Wu Z, Luo J (2018) Triiodide-induced band-edge reconstruction of a lead-free perovskite-derivative hybrid for strong light absorption. Chem Mater 30:4081–4088. https://doi.org/10.1021/acs.chemmater.8b01200
41. Bondi A (1964) van der Waals' volumes and radii. J Phys Chem 68:441–451. https://doi.org/10.1021/j100785a001
42. Wang P, Chen ZR, Li HH (2020) Novel viologen/iodobismuthate hybrids: structures, thermochromisms and theoretical calculations. J Cluster Sci 31:943–950. https://doi.org/10.1007/s10876-019-01699-1
43. James Z, Cai Y, Vaqueiro P (2021) Crystal structure of $(C_9H_{17}N_2)_3[Bi_2I_9]$. Acta Cryst E77:899–902. https://doi.org/10.1107/S2056989021007799
44. Louvain N, Mercier N, Boucher F (2009) α- to β-(dmes)BiI_5 (dmes = dimethyl(2-ethylammonium)sulfonium dication): umbrella reversal of sulfonium in the solid state and short I···I interchain contacts—crystal structures, optical properties, and theoretical investigations of 1D iodobismuthates. Inorg Chem 48:879–888. https://doi.org/10.1021/ic801900r
45. Kawai T, Shimanuki S (1993) Optical studies of $(CH_3NH_3)_3Bi_2I_9$ single crystals. Phys Status Solidi B 177:K43–K45. https://doi.org/10.1002/pssb.2221770128
46. Hrizi C, Trigui A, Abid Y, Chniba-Boudjada N, Bordet P, Chaabouni S (2011) *α*- to *β*-$[C_6H_4(NH_3)_2]_2Bi_2I_{10}$ reversible solid-state transition, thermochromic and optical studies in the *p*-phenylenediamine-based iodobismuthate(III) material. J Solid State Chem 184:3336–3344. https://doi.org/10.1016/j.jssc.2011.10.004
47. Kamminga ME, Stroppa A, Picozzi S, Chislov M, Zvereva IA, Baas J, Meetsma A, Blake GR, Palstra TTM (2017) Polar nature of $(CH_3NH_3)_3Bi_2I_9$ perovskite-like hybrids. Inorg Chem 56:33–41. https://doi.org/10.1021/acs.inorgchem.6b01699
48. Park BW, Philippe B, Zhang X, Rensmo H, Boschloo G, Johansson EMJ (2015) Bismuth based hybrid perovskites $A_3Bi_2I_9$ (A: methylammonium or cesium) for solar cell application. Adv Mater 27:6806–6813. https://doi.org/10.1002/adma.201501978
49. Ghasemi M, Lyu M, Roknuzzaman M, Yun JH, Hao M, He D, Bai Y, Chen P, Bernhardt PV, Ostrikov K, Wang L (2019) Phenethylammonium bismuth halides: from single crystals to bulky-organic cation promoted thin-film deposition for potential optoelectronic applications. J Mater Chem A 7:20733–20741. https://doi.org/10.1039/C9TA07454F
50. Zhang J, Han S, Ji C, Zhang W, Wang Y, Tao K, Sun Z, Luo J (2017) $[(CH_3)_3NH]_3Bi_2I_9$: a polar lead-free hybrid perovskite-like material as a potential semiconducting absorber. Chem Eur J 23:17304–17310. https://doi.org/10.1002/chem.201703346
51. García-Fernández A, Marcos-Cives I, Platas-Iglesias C, Castro-García S, Vázquez-García D, Fernández A, Sánchez-Andújar M (2018) Diimidazolium halobismuthates $[Dim]_2[Bi_2X_{10}]$ (X = Cl^-, Br^-, or I^-): a new class of thermochromic and photoluminescent materials. Inorg Chem 57:7655–7664. https://doi.org/10.1021/acs.inorgchem.8b00629
52. Li T, Wang Q, Nichol GS, Morrison CA, Han H, Hu Y, Robertson N (2018) Extending lead-free hybrid photovoltaic materials to new structures: thiazolium, aminothiazolium and imidazolium iodobismuthates. Dalton Trans 47:7050–7058. https://doi.org/10.1039/C8DT00864G
53. Möbs J, Gerhard M, Heine J (2020) $(HPy)_2(Py)CuBi_3I_{12}$, a low bandgap metal halide photoconductor. Dalton Trans 49:14397–14400. https://doi.org/10.1039/D0DT03427D

54. Möbs J, Luy JN, Shlyaykher A, Tonner R, Heine J (2021) The influence of copper on the optical band gap of heterometallic iodido antimonates and bismuthates. Dalton Trans 50:15855–15869. https://doi.org/10.1039/D1DT02828F

Authors and Affiliations

Yunhe Cai[1] · Ann M. Chippindale[1] · Paz Vaqueiro[1]

✉ Paz Vaqueiro
p.vaqueiro@reading.ac.uk

[1] Department of Chemistry, University of Reading, Whiteknights, Reading, Berkshire RG6 6DX, UK